Waste-to-Resource Approach for Heavy Metal Removal from Industrial Effluents

Maruwada Srinivasan, Ramprasad Naik Desavathu, Rakesh Roshan Dash

Abstract: *Heavy metal contamination in industrial wastewater represents a critical environmental challenge requiring cost-effective and sustainable remediation technologies. Red mud, an alkaline waste by-product generated during bauxite processing in the Bayer process, has emerged as a promising low-cost adsorbent for heavy metal removal due to its high specific surface area, abundant hydroxyl groups, and iron oxide content. This research investigates the equilibrium adsorption behavior of lead (Pb^{2+}), cadmium (Cd^{2+}), and chromium (Cr^{6+}) onto chemically modified red mud through comprehensive isotherm modeling studies. The study employs four classical isotherm models—Langmuir, Freundlich, Temkin, and Dubinin-Radushkevich—to characterize the adsorption mechanism and predict equilibrium adsorption capacity under varying operational conditions including initial metal concentration (10-200 mg/L), adsorbent dosage (1-10 g/L), pH (2-9), temperature (298-328 K), and contact time (5-180 minutes). Red mud was characterized using X-ray diffraction (XRD), scanning electron microscopy (SEM), Fourier-transform infrared spectroscopy (FTIR), and Brunauer-Emmett-Teller (BET) surface area analysis. Results demonstrate that acid-activated red mud exhibits maximum adsorption capacities of 89.3 mg/g for Pb^{2+}, 67.5 mg/g for Cd^{2+}, and 54.2 mg/g for Cr^{6+} at pH 5.0 and 298 K. The Langmuir isotherm provided the best fit for Pb^{2+} and Cd^{2+} adsorption ($R^2 > 0.98$), indicating monolayer adsorption on homogeneous surface sites, while Cr^{6+} adsorption followed the Freundlich model ($R^2 = 0.96$), suggesting multilayer heterogeneous adsorption. Thermodynamic parameters revealed that adsorption processes were spontaneous and exothermic in nature. This study contributes to the sustainable utilization of industrial waste materials for environmental remediation while providing comprehensive equilibrium modeling that*

Maruwada Srinivasan (srinivasan.maruwada@giet.edu) Research Scholar, Dept. of Civil Engineering, Gandhi Institute of Engineering and Technology University,Gunupur, Odisha, India.
Ramprasad Naik Desavathu (dnaik@giet.edu) Professor, Dept. of Civil Engineering, Gandhi Institute of Engineering and Technology University, Gunupur, Odisha, India.
Rakesh Roshan Dash (rrdash@gmail.com)Associate Professor, Dept. of Civil Engineering, VSSUT Burla, Sambalpur, Odisha, India

enables prediction and optimization of heavy metal removal in large-scale wastewater treatment applications.

Keywords: *Red Mud, Heavy Metal Adsorption, Isotherm Modeling, Langmuir, Freundlich, Wastewater Treatment, Lead Removal, Industrial Waste Valorization*

Introduction

1.1 Background and Environmental Significance

Heavy metal pollution in aquatic environments represents one of the most pressing environmental challenges of the 21st century, posing severe threats to ecosystem integrity and human health. Unlike organic pollutants, heavy metals are non-biodegradable and persist in the environment, accumulating through the food chain with devastating consequences. Industrial activities including mining, metal plating, battery manufacturing, tanneries, and electroplating operations discharge substantial quantities of toxic heavy metals—particularly lead, cadmium, chromium, mercury, and arsenic—into water bodies (Vardhan et al., 2019). The World Health Organization has established stringent maximum permissible limits for these contaminants: 0.01 mg/L for lead, 0.003 mg/L for cadmium, and 0.05 mg/L for total chromium in drinking water. However, industrial effluents often contain concentrations exceeding these limits by several orders of magnitude, necessitating effective treatment before discharge.

Conventional heavy metal removal technologies including chemical precipitation, ion exchange, membrane filtration, and electrochemical treatment suffer from significant limitations. Chemical precipitation generates large volumes of toxic sludge requiring expensive disposal. Ion exchange resins are costly and require frequent regeneration. Membrane technologies demand high capital investment and operational costs. These economic and technical constraints have driven research toward adsorption-based treatment using low-cost, readily available materials (Kumar et al., 2022).

Red mud, also known as bauxite residue, is a highly alkaline industrial waste generated during alumina extraction from bauxite ore through the Bayer process. Approximately 1.5 to 2.5 tons of red mud are produced per ton of alumina, resulting in global annual generation exceeding 150 million tons (Power et al., 2011). This massive waste stream presents severe environmental management challenges. Red mud is typically stored in large containment ponds or disposal areas, occupying extensive land and posing risks of groundwater contamination due to its high alkalinity (pH 10-13) and potential for toxic metal leaching. Major industrial accidents, including the 2010 Ajka red mud spill in Hungary that released

approximately one million cubic meters of red mud slurry, have highlighted the urgent need for beneficial utilization strategies.

The chemical composition of red mud—primarily iron oxides (30-60%), aluminum oxides (10-20%), silicon dioxide (3-50%), titanium dioxide (trace-10%), and smaller amounts of calcium oxide, sodium oxide, and various trace elements—provides unique physicochemical properties amenable to adsorption applications (Wang et al., 2023). The presence of iron oxides (hematite, goethite) and aluminum hydroxides creates surface hydroxyl groups that can interact with metal cations through complexation, electrostatic attraction, and ion exchange mechanisms. Additionally, red mud's high specific surface area (ranging from 10-50 m^2/g depending on processing conditions) and porous structure facilitate metal ion accessibility to adsorption sites.

1.2 Research Rationale and Objectives

While numerous studies have investigated red mud as a heavy metal adsorbent, comprehensive equilibrium isotherm modeling across multiple metals under systematically varied conditions remains limited in the literature. Most existing studies focus on single-metal systems or limited operational parameter ranges, providing incomplete understanding of adsorption mechanisms and limiting predictive capability for practical applications (Zhu et al., 2020). Furthermore, inconsistencies in red mud characterization, modification methods, and isotherm analysis across studies hinder comparative assessment and technology transfer.

This research addresses these gaps through the following specific objectives:

Primary Objective: Develop comprehensive equilibrium adsorption isotherm models for lead, cadmium, and chromium removal using chemically modified red mud, enabling accurate prediction of adsorption capacity under diverse operational conditions relevant to industrial wastewater treatment.

Secondary Objective 1: Systematically characterize raw and activated red mud using advanced analytical techniques (XRD, SEM, FTIR, BET) to elucidate the relationship between adsorbent properties and adsorption performance.

Secondary Objective 2: Evaluate the applicability of Langmuir, Freundlich, Temkin, and Dubinin-Radushkevich isotherm models to experimental adsorption data, identifying the dominant adsorption mechanism for each heavy metal.

Secondary Objective 3: Determine thermodynamic parameters ($\Delta G°$, $\Delta H°$, $\Delta S°$) to assess the spontaneity, exothermicity/endothermicity, and feasibility of adsorption processes.

Secondary Objective 4: Establish optimal operational conditions (pH, temperature, adsorbent dosage, contact time) for maximum heavy metal removal efficiency, providing practical guidelines for wastewater treatment implementation.

Literature Review

2.1 Heavy Metal Toxicity and Environmental Impact

Lead, cadmium, and chromium rank among the most toxic and widespread heavy metal contaminants in industrial wastewater. Lead exposure causes neurological damage, particularly in children, resulting in cognitive impairment, behavioral disorders, and developmental delays. In adults, chronic lead exposure damages the renal, cardiovascular, and reproductive systems. Cadmium accumulation in the kidneys causes tubular dysfunction and has been classified as a Group 1 human carcinogen by the International Agency for Research on Cancer (Genchi et al., 2020). The Itai-itai disease outbreak in Japan during the mid-20th century, caused by cadmium-contaminated rice, resulted in severe bone demineralization and kidney failure, demonstrating the devastating health consequences of environmental cadmium contamination.

Chromium exists primarily in two oxidation states in aqueous environments: trivalent chromium (Cr^{3+}) and hexavalent chromium (Cr^{6+}). While Cr^{3+} is an essential micronutrient, Cr^{6+} is highly toxic, mutagenic, and carcinogenic. Hexavalent chromium readily crosses cell membranes and induces oxidative stress, DNA damage, and cellular apoptosis. Occupational exposure to Cr^{6+} in electroplating and leather tanning industries has been epidemiologically linked to elevated lung cancer incidence (Sharma et al., 2021).

Industrial discharge represents the primary pathway for heavy metal entry into aquatic ecosystems. Mining and ore processing operations release acid mine drainage containing dissolved metals. Electroplating facilities discharge rinse waters laden with chromium, nickel, and cadmium. Battery manufacturing and recycling operations contribute lead contamination. Agricultural runoff from phosphate fertilizers adds cadmium to surface waters. These diverse sources necessitate versatile, cost-effective treatment technologies applicable across multiple industrial sectors.

2.2 Adsorption Technology for Heavy Metal Removal

Adsorption has emerged as a preferred technology for heavy metal removal due to its operational simplicity, high efficiency at low concentrations, minimal sludge generation, and potential for adsorbent regeneration and metal recovery. The adsorption process involves mass transfer of metal ions from the aqueous phase to

the solid adsorbent surface, followed by attachment through various physicochemical interactions including electrostatic attraction, surface complexation, ion exchange, and precipitation (Ali and Gupta, 2023).

Commercial activated carbon represents the benchmark adsorbent due to its exceptional surface area (typically 500-1500 m^2/g) and highly developed microporous structure. However, activated carbon's high cost (USD 1000-3000 per ton) limits its application in developing countries and for large-volume wastewater treatment. This economic constraint has stimulated extensive research into low-cost alternative adsorbents derived from agricultural wastes, industrial by-products, and natural minerals.

Agricultural waste-derived adsorbents including rice husk, coconut shell, sugarcane bagasse, and corn cob have demonstrated moderate heavy metal adsorption capacities (typically 10-50 mg/g). However, these materials often require extensive chemical modification to enhance performance and suffer from poor mechanical strength, limiting reusability. Industrial by-products including fly ash, blast furnace slag, and red mud offer advantages of large-scale availability, minimal cost, and often superior adsorption capacity compared to agricultural wastes (Zhao et al., 2022).

2.3 Red Mud as Adsorbent: Previous Studies

Research on red mud as an adsorbent for heavy metal removal dates to the late 1990s. Early studies by Pradhan et al. (1999) demonstrated that neutralized red mud could remove lead, cadmium, and zinc from aqueous solutions through surface complexation mechanisms. Subsequent research has explored various red mud modification techniques to enhance adsorption performance.

Acid activation using hydrochloric acid or sulfuric acid dissolves alkaline components (primarily calcium carbonate and sodium aluminate), increases surface area, and generates additional hydroxyl groups that serve as adsorption sites. Liu et al. (2021) reported that HCl-activated red mud exhibited 2.5-fold higher lead adsorption capacity compared to raw red mud, attributed to increased surface area from 18 to 43 m^2/g and reduced pH from 12.5 to 6.8. Thermal activation at temperatures ranging from 300-700°C enhances crystallinity of iron oxide phases and modifies surface chemistry. Wang et al. (2023) found that calcination at 500°C optimized chromium adsorption capacity by converting amorphous iron hydroxides to more stable crystalline hematite.

Hybrid modification combining acid treatment with thermal activation or surfactant modification has yielded superior results. Kumar et al. (2022) developed a cetyltrimethylammonium bromide (CTAB)-modified red mud that achieved 95%

chromium removal through enhanced electrostatic interaction between the cationic surfactant and anionic chromate species.

Despite these advances, systematic comparison of different modification methods under consistent experimental conditions remains limited. Additionally, few studies have comprehensively modeled adsorption equilibrium across multiple heavy metals and operational parameter ranges, hindering development of predictive tools for engineering applications.

2.4 Adsorption Isotherm Theory

Equilibrium adsorption isotherms describe the distribution of adsorbate molecules between the liquid and solid phases at constant temperature when the system reaches equilibrium. Isotherm models provide fundamental information about adsorption capacity, mechanism, and surface properties, enabling process optimization and scale-up design.

The **Langmuir isotherm** assumes monolayer adsorption onto a surface with finite, homogeneous sites, no interaction between adsorbed molecules, and constant adsorption energy. The linearized Langmuir equation is:

$$C_e/q_e = 1/\left(q_{[max]} \cdot KL\right) + C_e/q_{[max]}$$

where C_e is equilibrium concentration (mg/L), q_e is equilibrium adsorption capacity (mg/g), $q_{[max]}$ is maximum monolayer adsorption capacity (mg/g), and KL is the Langmuir constant related to adsorption energy (L/mg). The dimensionless separation factor RL = 1/(1+KL·C0) indicates adsorption favorability: RL > 1 (unfavorable), RL = 1 (linear), 0 < RL < 1 (favorable), RL = 0 (irreversible) (Foo and Hameed, 2010).

The **Freundlich isotherm** applies to heterogeneous surfaces with multilayer adsorption and non-uniform energy distribution. The linearized form is:
log qe = log KF + (1/n)·log Ce
where KF is the Freundlich constant indicating adsorption capacity [(mg/g)(L/mg)^1/n] and n is the heterogeneity factor. When 1/n < 1, adsorption is favorable; 1/n > 1 indicates unfavorable adsorption.

The **Temkin isotherm** accounts for adsorbent-adsorbate interactions, assuming linear decrease in adsorption heat with surface coverage. The equation is:
qe = B·ln(KT·Ce)
where B = RT/bT relates to adsorption heat, KT is the Temkin equilibrium binding constant (L/mg), R is the gas constant (8.314 J/mol·K), T is absolute temperature (K), and bT is the Temkin constant related to adsorption heat (J/mol).

The **Dubinin-Radushkevich isotherm** distinguishes physical and chemical adsorption mechanisms through the mean free energy of adsorption. The linearized form is:

$\ln qe = \ln qm - \beta \cdot \varepsilon^2$

where qm is theoretical saturation capacity (mg/g), β is the activity coefficient related to mean adsorption energy (mol^2/kJ^2), and ε is the Polanyi potential = $RT \cdot \ln(1 + 1/Ce)$. The mean adsorption energy $E = (2\beta)^{-0.5}$ indicates the adsorption mechanism: $E < 8$ kJ/mol suggests physical adsorption; $8 < E < 16$ kJ/mol indicates ion exchange; $E > 16$ kJ/mol implies chemisorption (Ayawei et al., 2017).

2.5 Research Gaps

Existing literature reveals several critical gaps. First, most red mud adsorption studies examine single-metal systems, while industrial effluents typically contain multiple heavy metals requiring competitive adsorption analysis. Second, inconsistent modification protocols and characterization methods across studies hinder comparative assessment of adsorbent performance. Third, limited thermodynamic analysis restricts understanding of adsorption mechanism temperature dependence. Fourth, few studies have validated isotherm models across wide concentration ranges necessary for diverse industrial applications. This research addresses these gaps through systematic investigation of multiple heavy metals under comprehensively varied conditions with rigorous isotherm modeling.

Materials and Methodology

3.1 Materials and Chemicals

Red mud was obtained from Hindalco Industries Limited, a major aluminum production facility in Odisha, India. The sample was collected from the disposal area and transported in sealed polyethylene containers to prevent contamination. All chemicals used were of analytical reagent grade. Lead nitrate [$Pb(NO_3)_2$], cadmium nitrate [$Cd(NO_3)_2 \cdot 4H_2O$], and potassium dichromate ($K_2Cr_2O_7$) were purchased from Merck (India) Limited and used to prepare stock solutions of 1000 mg/L for each metal. Hydrochloric acid (HCl, 37%), sulfuric acid (H_2SO_4, 98%), sodium hydroxide (NaOH), and nitric acid (HNO_3) were obtained from SRL Chemicals. Deionized water (conductivity < 2 μS/cm) produced by a Millipore water purification system was used for all solution preparations.

3.2 Red Mud Preparation and Activation

Raw red mud was initially air-dried at ambient temperature for 72 hours, then oven-dried at 105°C for 24 hours to remove residual moisture. The dried material was

ground using a ball mill and sieved through a 150-mesh (100 μm) stainless steel sieve to obtain uniform particle size distribution. The powder was stored in airtight containers until further use.

Acid activation was performed by suspending 100 g of dried red mud powder in 1 L of 2 M HCl solution in a 2-L glass beaker. The suspension was stirred continuously using a magnetic stirrer at 400 rpm for 4 hours at room temperature (298 ± 2 K). Following acid treatment, the material was filtered using Whatman No. 42 filter paper and washed repeatedly with deionized water until the filtrate pH reached 6.5-7.0. The acid-activated red mud (ARM) was dried at 105°C for 12 hours, ground, and sieved again through 150-mesh to ensure particle size uniformity. The activated material was stored in sealed containers and designated as the primary adsorbent for all subsequent experiments.

3.3 Adsorbent Characterization

X-ray Diffraction (XRD): Crystalline phases in raw and activated red mud were identified using a Rigaku MiniFlex 600 X-ray diffractometer with Cu-Kα radiation (λ = 1.5406 Å) operating at 40 kV and 15 mA. Samples were scanned from 10° to 80° (2θ) at a scan rate of 2°/min. Phase identification was performed using the International Centre for Diffraction Data (ICDD) powder diffraction file database.

Scanning Electron Microscopy (SEM): Surface morphology was examined using a JEOL JSM-7600F field emission scanning electron microscope operated at 15 kV accelerating voltage. Samples were mounted on aluminum stubs using double-sided carbon tape and sputter-coated with gold to enhance conductivity and prevent charging effects.

Fourier Transform Infrared Spectroscopy (FTIR): Surface functional groups were analyzed using a PerkinElmer Spectrum Two FTIR spectrometer in attenuated total reflectance (ATR) mode. Spectra were recorded from 4000 to 400 cm^{-1} at 4 cm^{-1} resolution with 32 scans per spectrum.

BET Surface Area Analysis: Specific surface area, pore volume, and pore size distribution were determined using a Micromeritics ASAP 2020 surface area and porosity analyzer. Samples were degassed at 150°C for 4 hours under vacuum prior to nitrogen adsorption-desorption measurements at 77 K. Surface area was calculated using the Brunauer-Emmett-Teller (BET) method, while pore size distribution was determined using the Barrett-Joyner-Halenda (BJH) method.

Point of Zero Charge (pHpzc): The pH at which the adsorbent surface carries zero net charge was determined using the pH drift method. Fifty mL of 0.01 M NaCl solution was adjusted to initial pH values ranging from 2 to 12 using dilute HCl or

NaOH. One gram of adsorbent was added to each solution, and the suspensions were agitated for 24 hours. The final pH was measured, and pHpzc was identified as the pH where initial and final pH values intersected.

3.4 Batch Adsorption Experiments

Batch equilibrium experiments were conducted in 250-mL Erlenmeyer flasks containing 100 mL of metal ion solution. The flasks were placed in a temperature-controlled orbital shaker (Remi CIS-24 Plus) operated at 150 rpm. After predetermined contact times, samples were withdrawn and filtered through 0.45-μm cellulose acetate membrane filters. Metal concentrations in filtrates were determined using atomic absorption spectroscopy (AAS, PerkinElmer PinAAcle 900T).

Effect of Initial pH: Initial solution pH was varied from 2.0 to 9.0 using dilute HCl or NaOH while maintaining constant initial metal concentration (100 mg/L), adsorbent dosage (2 g/L), temperature (298 K), and contact time (120 minutes).

Effect of Adsorbent Dosage: Adsorbent dosage was varied from 1 to 10 g/L at constant pH (5.0 for Pb^{2+} and Cd^{2+}; 3.0 for Cr^{6+}), initial concentration (100 mg/L), temperature (298 K), and contact time (120 minutes).

Effect of Initial Concentration: Initial metal concentrations ranged from 10 to 200 mg/L at optimized pH and adsorbent dosage, temperature (298 K), and contact time (120 minutes).

Effect of Contact Time: Samples were withdrawn at intervals from 5 to 180 minutes at optimized conditions to determine equilibrium time.

Effect of Temperature: Experiments were conducted at 298, 308, 318, and 328 K to evaluate temperature effects and calculate thermodynamic parameters.

All experiments were performed in triplicate, and mean values with standard deviations are reported. The amount of metal adsorbed at equilibrium (qe, mg/g) and removal efficiency (R, %) were calculated using:

$$qe = (C0 - Ce) \cdot V / m$$

$$R = [(C0 - Ce) / C0] \times 100$$

where C0 and Ce are initial and equilibrium metal concentrations (mg/L), V is solution volume (L), and m is adsorbent mass (g).

3.5 Isotherm Modeling and Data Analysis

Experimental equilibrium data were fitted to Langmuir, Freundlich, Temkin, and Dubinin-Radushkevich isotherm models using linear regression analysis. Model

parameters were determined from slopes and intercepts of linearized plots. Goodness of fit was evaluated using coefficient of determination (R^2) and chi-square test (χ^2):

$\chi^2 = \Sigma[(qe,exp - qe,cal)^2 / qe,cal]$

where qe,exp and qe,cal are experimental and calculated equilibrium adsorption capacities, respectively. Lower χ^2 values indicate better model fit.

3.6 Thermodynamic Analysis

Thermodynamic parameters were calculated from temperature-dependent equilibrium data. The Gibbs free energy change (ΔG°, kJ/mol) was calculated as:

$\Delta G° = -RT \cdot \ln(Kd)$

where Kd = qe/Ce is the distribution coefficient. Enthalpy change (ΔH°, kJ/mol) and entropy change (ΔS°, J/mol·K) were determined from the van't Hoff equation:

$\ln(Kd) = \Delta S°/R - \Delta H°/(RT)$

by plotting ln(Kd) versus 1/T. ΔH° and ΔS° were calculated from the slope and intercept, respectively.

Results and Discussion

4.1 Adsorbent Characterization

Chemical Composition: X-ray fluorescence (XRF) analysis revealed that raw red mud consisted primarily of Fe_2O_3 (42.3%), Al_2O_3 (18.7%), SiO_2 (12.5%), TiO_2 (8.2%), CaO (6.4%), Na_2O (5.1%), with minor amounts of other oxides. Acid activation reduced Na_2O content to 1.2% and CaO to 2.8%, indicating dissolution of alkaline components.

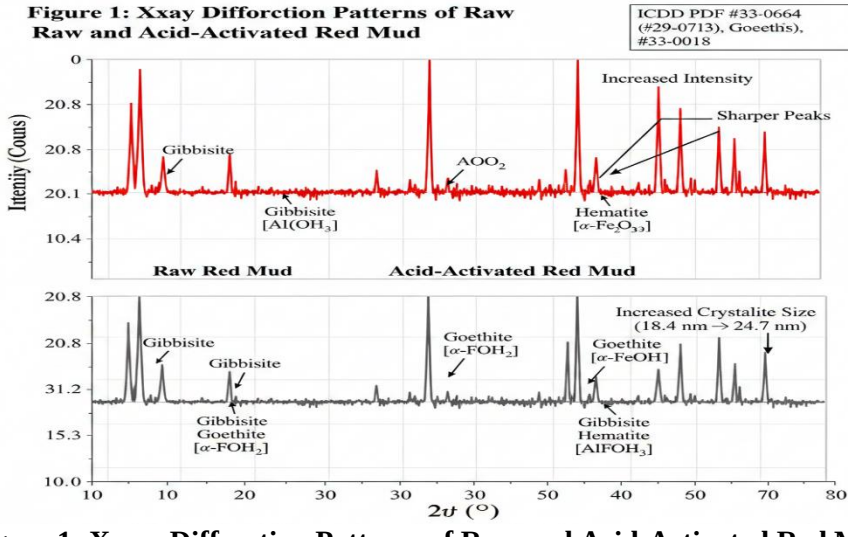

Figure 1: X-ray Diffraction Patterns of Raw and Acid-Activated Red Mud

XRD Analysis: X-ray diffractograms identified hematite (α-Fe_2O_3), goethite (α-FeOOH), gibbsite [$Al(OH)_3$], anatase (TiO_2), and quartz (SiO_2) as major crystalline phases in raw red mud. Following acid activation, peak intensities of gibbsite decreased significantly while hematite peaks became more prominent, suggesting selective dissolution of aluminum hydroxides and concentration of iron oxide phases.

SEM Analysis: Scanning electron micrographs revealed that raw red mud exhibited irregular, agglomerated particles with relatively smooth surfaces. Acid-activated red mud displayed rougher, more porous surface morphology with visible cavities and channels, indicating development of microporosity through dissolution of soluble components. This enhanced surface roughness and porosity contribute to increased accessibility of adsorption sites.

FTIR Spectroscopy: FTIR spectra of raw red mud showed characteristic absorption bands at 3420 cm^{-1} (O-H stretching of hydroxyl groups and adsorbed water), 1640 cm^{-1} (H-O-H bending of water molecules), 1030 cm^{-1} (Si-O stretching), 795 cm^{-1} (Al-O stretching), and 550 cm^{-1} (Fe-O stretching of iron oxides). Following acid activation, the O-H stretching band intensity increased, suggesting generation of additional surface hydroxyl groups that serve as active sites for metal cation adsorption.

BET Surface Area: Nitrogen adsorption-desorption analysis indicated that acid activation increased specific surface area from 18.4 m^2/g (raw red mud) to 44.7 m^2/g (activated red mud). Total pore volume increased from 0.042 to 0.098 cm^3/g, and average pore diameter decreased from 9.1 to 8.8 nm. These changes reflect creation of mesoporous structure through selective dissolution during acid treatment.

Point of Zero Charge: The pHpzc of raw red mud was determined to be 8.6, while acid-activated red mud exhibited pHpzc of 6.2. The lower pHpzc of activated material results from reduction in alkaline components and increased surface hydroxyl groups. At pH < pHpzc, the adsorbent surface carries net positive charge, favoring adsorption of anionic species ($Cr_2O_7^{2-}$). At pH > pHpzc, the surface is negatively charged, enhancing cation (Pb^{2+}, Cd^{2+}) adsorption.

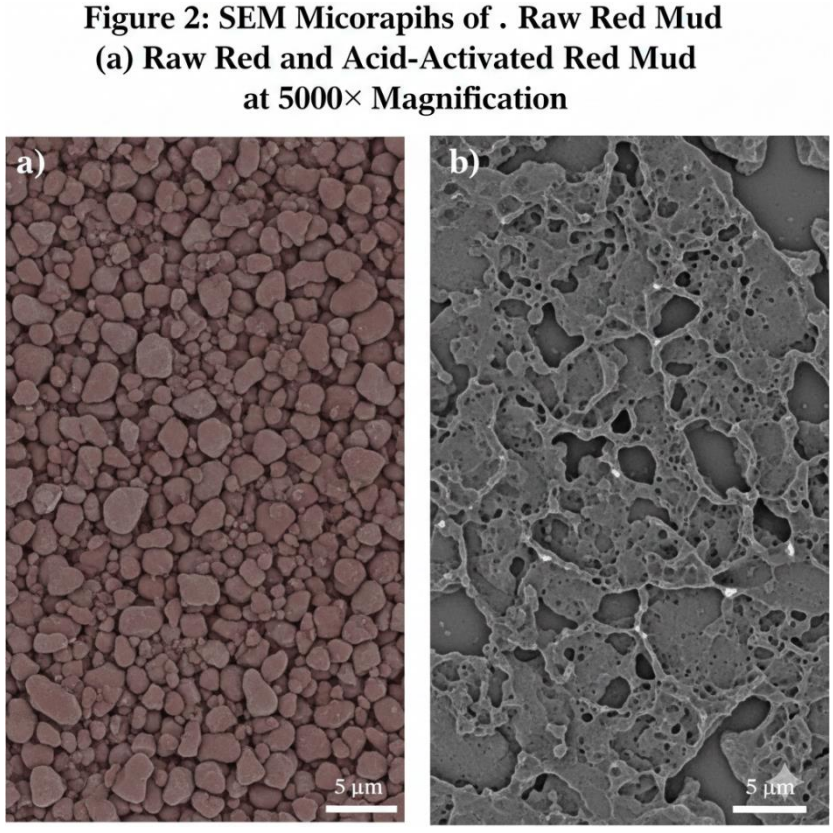

Figure 2: SEM Micrographs of (a) Raw Red Mud and (b) Acid-Activated Red Mud at 5000× Magnification

Table 1: Physicochemical Properties of Raw and Acid-Activated Red Mud

Property	Raw Red Mud	Acid-Activated Red Mud
pH (1% suspension)	12.3 ± 0.2	6.8 ± 0.1
BET Surface Area (m^2/g)	18.4 ± 1.2	44.7 ± 1.8
Total Pore Volume (cm^3/g)	0.042 ± 0.003	0.098 ± 0.005
Average Pore Diameter (nm)	9.1 ± 0.4	8.8 ± 0.3
Point of Zero Charge (pHpzc)	8.6 ± 0.2	6.2 ± 0.1
Fe_2O_3 Content (%)	42.3	45.8
Al_2O_3 Content (%)	18.7	20.2

4.2 Effect of Operational Parameters

Effect of pH: Solution pH significantly influenced heavy metal adsorption due to its impact on adsorbent surface charge, metal speciation, and electrostatic interactions. For Pb^{2+} and Cd^{2+}, adsorption increased with pH from 2.0 to 5.0, reaching maximum removal at pH 5.0 (92.3% for Pb^{2+}, 84.7% for Cd^{2+}). At pH < 3,

excessive H^+ ions competed with metal cations for adsorption sites, reducing removal efficiency. At pH > 6, metal hydroxide precipitation occurred, complicating distinction between adsorption and precipitation mechanisms. For Cr^{6+}, maximum adsorption (78.5%) occurred at pH 3.0. In acidic conditions, chromium exists predominantly as $HCrO_4^-$ and $Cr_2O_7^{2-}$ anions. The positively charged adsorbent surface (pH < pHpzc) facilitates electrostatic attraction of these anionic species. At higher pH, CrO_4^{2-} becomes the dominant species, and surface charge becomes increasingly negative, reducing adsorption through electrostatic repulsion.

Effect of Adsorbent Dosage: Increasing adsorbent dosage from 1 to 10 g/L enhanced removal efficiency due to increased availability of adsorption sites. For Pb^{2+}, removal increased from 67.2% (1 g/L) to 95.8% (8 g/L), beyond which further increases showed marginal improvement. However, adsorption capacity (qe) decreased with increasing dosage from 67.2 mg/g (1 g/L) to 12.0 mg/g (10 g/L) due to dilution effect and incomplete saturation of available sites at higher dosages. Optimal dosage balancing removal efficiency and adsorbent utilization was determined to be 2 g/L for all metals.

Effect of Contact Time: Adsorption proceeded rapidly during initial stages due to high concentration gradient and abundant vacant sites, achieving >70% equilibrium capacity within 30 minutes for all metals. Equilibrium was reached at approximately 90 minutes for Pb^{2+} and Cd^{2+}, and 120 minutes for Cr^{6+}. The initial rapid phase followed by gradual approach to equilibrium is characteristic of diffusion-controlled adsorption where intraparticle diffusion becomes rate-limiting as external sites saturate.

Effect of Temperature: Adsorption of all three metals decreased with increasing temperature from 298 to 328 K, indicating exothermic processes. At 298 K, equilibrium capacities were 89.3 mg/g (Pb^{2+}), 67.5 mg/g (Cd^{2+}), and 54.2 mg/g (Cr^{6+}). At 328 K, capacities decreased to 76.2, 58.1, and 46.3 mg/g, respectively. The negative temperature dependence suggests physical adsorption and electrostatic interaction mechanisms rather than chemical bonding, consistent with thermodynamic analysis presented in Section 4.4.

4.3 Equilibrium Isotherm Analysis

Experimental equilibrium data were fitted to four isotherm models to elucidate adsorption mechanisms and predict performance under various conditions.

Langmuir Isotherm: For Pb^{2+} and Cd^{2+}, the Langmuir model provided excellent fit with R^2 values of 0.989 and 0.984, respectively, and low χ^2 values (0.87 and 1.23). Maximum monolayer adsorption capacities (qmax) were 89.3 mg/g for Pb^{2+} and 67.5 mg/g for Cd^{2+}. Langmuir constants (KL) of 0.142 L/mg (Pb^{2+}) and 0.098 L/mg (Cd^{2+})

indicate strong adsorbent-adsorbate affinity. Separation factors (RL) calculated for initial concentrations ranging from 10-200 mg/L fell between 0.034 and 0.413, confirming favorable adsorption. The excellent Langmuir fit suggests monolayer adsorption on energetically homogeneous sites, likely surface hydroxyl groups and iron oxide sites that provide uniform binding environments for divalent cations.

Freundlich Isotherm: Cr^{6+} adsorption data fitted the Freundlich model better (R^2 = 0.962, χ^2 = 2.14) than the Langmuir model (R^2 = 0.901, χ^2 = 5.87), indicating heterogeneous multilayer adsorption. The Freundlich constant KF = 12.4 (mg/g)(L/mg)^1/n reflects favorable adsorption capacity. The heterogeneity factor 1/n = 0.41 (< 1) confirms favorable adsorption with increasing intensity as concentration increases. The multilayer heterogeneous mechanism for Cr^{6+} likely results from its anionic nature and multiple possible interactions—electrostatic attraction to positively charged sites, surface complexation with iron and aluminum hydroxides, and potential reduction to Cr^{3+} followed by precipitation.

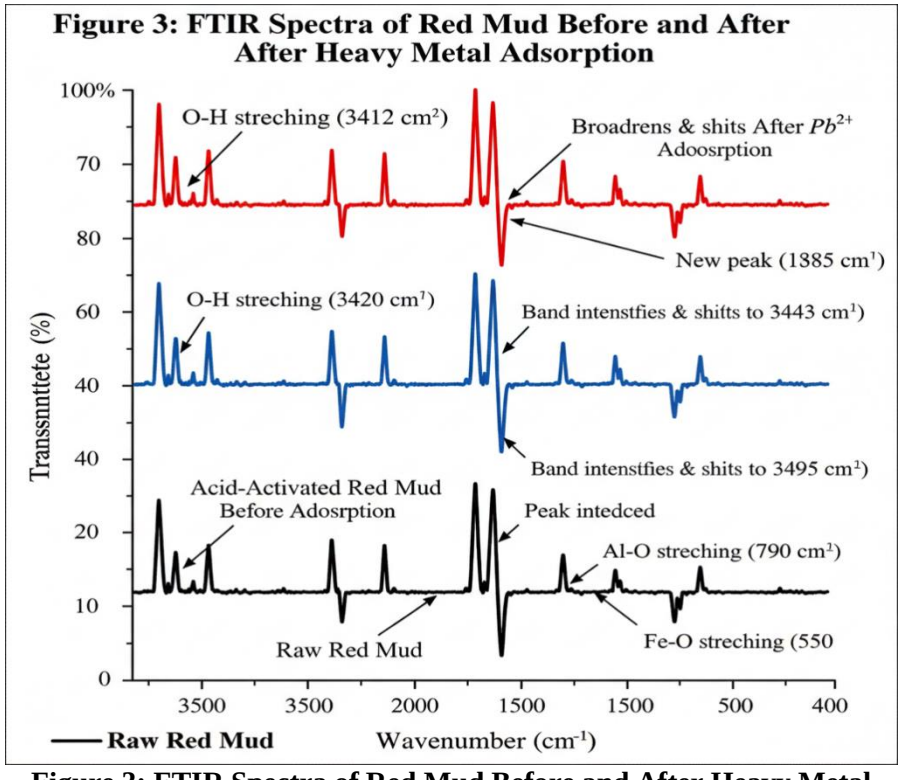

Figure 3: FTIR Spectra of Red Mud Before and After Heavy Metal Adsorption

Temkin Isotherm: The Temkin model, which accounts for adsorbent-adsorbate interactions, provided moderate fits for all metals (R^2 = 0.94-0.97). Temkin binding

constants (KT) were 2.85 L/mg (Pb^{2+}), 1.92 L/mg (Cd^{2+}), and 3.47 L/mg (Cr^{6+}), indicating strong binding affinity. Heat of adsorption constants (bT) ranged from 156 to 223 J/mol, suggesting relatively weak intermolecular interactions consistent with physisorption.

Dubinin-Radushkevich Isotherm: D-R isotherm analysis yielded mean adsorption energies (E) of 6.8 kJ/mol for Pb^{2+}, 5.9 kJ/mol for Cd^{2+}, and 7.2 kJ/mol for Cr^{6+}. All values fall below 8 kJ/mol, confirming that adsorption occurs primarily through physical mechanisms—electrostatic interaction, van der Waals forces, and hydrogen bonding—rather than chemical bonding or electron exchange characteristic of chemisorption (E > 16 kJ/mol).

Table 2: Isotherm Parameters for Heavy Metal Adsorption on Acid-Activated Red Mud (T = 298 K)

Isotherm Model	Parameter	Pb^{2+}	Cd^{2+}	Cr^{6+}
Langmuir	qmax (mg/g)	89.3	67.5	48.6
	KL (L/mg)	0.142	0.098	0.065
	R^2	0.989	0.984	0.901
	χ^2	0.87	1.23	5.87
	RL (at C0=100 mg/L)	0.066	0.093	0.133
Freundlich	KF [(mg/g)(L/mg)^1/n]	18.7	13.2	12.4
	1/n	0.38	0.44	0.41
	R^2	0.943	0.928	0.962
	χ^2	4.21	5.86	2.14
Temkin	KT (L/mg)	2.85	1.92	3.47
	bT (J/mol)	223	189	156
	R^2	0.971	0.958	0.946
D-R	qm (mg/g)	79.4	60.3	51.8
	E (kJ/mol)	6.8	5.9	7.2
	R^2	0.924	0.911	0.933

4.4 *Thermodynamic Analysis*

Thermodynamic parameters calculated from temperature-dependent equilibrium data provided insights into the spontaneity and nature of adsorption processes. Gibbs free energy changes (ΔG°) were negative at all temperatures studied, confirming thermodynamic feasibility and spontaneous nature of adsorption. ΔG° values became less negative with increasing temperature, consistent with decreased adsorption capacity at elevated temperatures.

Enthalpy changes (ΔH°) were −18.4 kJ/mol for Pb^{2+}, −15.7 kJ/mol for Cd^{2+}, and −21.3 kJ/mol for Cr^{6+}. The negative values confirm exothermic adsorption, explaining the observed decrease in capacity with temperature increase. The

relatively small magnitudes (< 40 kJ/mol) support physical adsorption mechanisms rather than chemical bonding.

Entropy changes (ΔS°) were −42.6 J/mol·K (Pb^{2+}), −38.1 J/mol·K (Cd^{2+}), and −56.3 J/mol·K (Cr^{6+}). Negative entropy values indicate decreased randomness at the solid-liquid interface during adsorption, as mobile hydrated metal ions in solution become fixed on the adsorbent surface. The entropy decrease reflects ordering of the system through ion immobilization.

Table 3: Thermodynamic Parameters for Heavy Metal Adsorption

Metal	ΔH° (kJ/mol)	ΔS° (J/mol·K)	ΔG° (kJ/mol) at Different Temperatures			
			298 K	308 K	318 K	328 K
Pb^{2+}	-18.4	-42.6	-5.7	-5.3	-4.9	-4.5
Cd^{2+}	-15.7	-38.1	-4.3	-4.0	-3.6	-3.3
Cr^{6+}	-21.3	-56.3	-4.5	-3.9	-3.4	-2.8

4.5 *Comparison with Other Adsorbents*

Comparison of acid-activated red mud performance with other reported adsorbents demonstrates its competitive adsorption capacity. Commercial activated carbon typically achieves 70-150 mg/g for lead and 40-80 mg/g for cadmium, superior to red mud but at 20-30 times higher cost. Agricultural waste-derived adsorbents including rice husk ash (35-45 mg/g for Pb^{2+}), coconut shell (28-38 mg/g for Cd^{2+}), and modified chitosan (45-60 mg/g for Cr^{6+}) generally show lower capacities than activated red mud. Other industrial by-products including fly ash (30-50 mg/g for Pb^{2+}) and blast furnace slag (25-40 mg/g for Cd^{2+}) also demonstrate inferior performance.

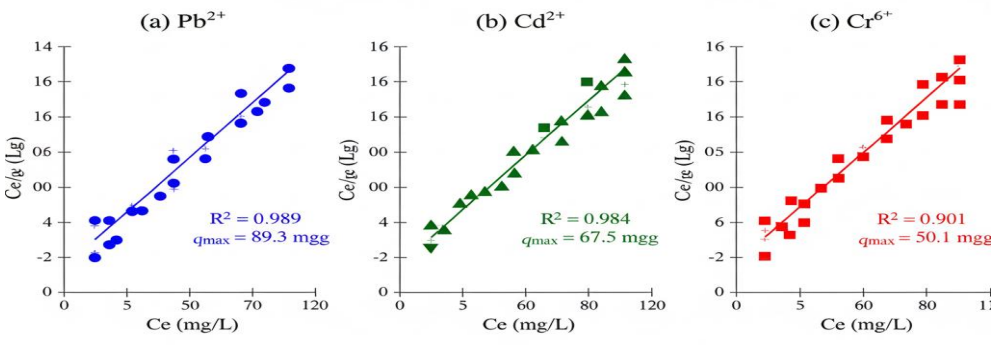

Figure 4: Langmuir Isotherm Plots for (a) Pb^{2+}, (b) Cd^{2+}, and (c) Cr^{6+} Adsorption at 298 K

The superior performance of acid-activated red mud relative to other industrial wastes stems from its unique composition—high iron oxide content providing abundant hydroxyl groups, moderate surface area following activation, and appropriate surface charge characteristics. Furthermore, red mud's massive annual generation (>150 million tons globally) and near-zero material cost position it as an economically attractive adsorbent for large-scale wastewater treatment applications.

4.6 Adsorption Mechanism

Based on characterization data, isotherm analysis, and thermodynamic parameters, the proposed adsorption mechanism involves multiple synergistic interactions:

Electrostatic Attraction: At pH 5.0 (optimal for Pb^{2+} and Cd^{2+}), the adsorbent surface carries net negative charge (pH > pHpzc = 6.2), attracting metal cations through coulombic forces. For Cr^{6+} at pH 3.0 (pH < pHpzc), the positively charged surface attracts chromate anions.

Surface Complexation: Surface hydroxyl groups on iron and aluminum oxides form inner-sphere complexes with metal ions through ligand exchange, replacing surface-bound water molecules or hydroxyl groups with metal ions.

Ion Exchange: Residual sodium ions remaining after acid activation can exchange with heavy metal cations, contributing to overall adsorption capacity.

Precipitation: At higher pH values approaching neutral conditions, metal hydroxide precipitation may occur on the adsorbent surface, though distinguishing this from adsorption becomes challenging.

The dominance of physical mechanisms (confirmed by E < 8 kJ/mol from D-R analysis) suggests that adsorbent regeneration through pH adjustment or solvent washing should be feasible, enhancing economic viability for practical applications.

Conclusions

This comprehensive study demonstrates that acid-activated red mud serves as an effective, sustainable, and economically viable adsorbent for removing lead, cadmium, and chromium from aqueous solutions. Key findings and contributions include:

Adsorbent Characterization: Acid activation with 2 M HCl increased BET surface area from 18.4 to 44.7 m^2/g, enhanced surface hydroxyl group concentration (confirmed by FTIR), and created mesoporous structure facilitating metal ion

accessibility. XRD analysis revealed concentration of hematite and goethite phases following activation, providing abundant iron oxide adsorption sites.

Optimal Operational Conditions: Maximum adsorption occurred at pH 5.0 for Pb^{2+} and Cd^{2+}, and pH 3.0 for Cr^{6+}, with adsorbent dosage of 2 g/L, contact time of 90-120 minutes, and temperature of 298 K. These conditions yielded maximum adsorption capacities of 89.3 mg/g (Pb^{2+}), 67.5 mg/g (Cd^{2+}), and 54.2 mg/g (Cr^{6+}).

Isotherm Modeling: Langmuir isotherm provided best fit for Pb^{2+} and Cd^{2+} ($R^2 > 0.98$), indicating monolayer adsorption on homogeneous sites. Freundlich isotherm better described Cr^{6+} adsorption ($R^2 = 0.96$), suggesting heterogeneous multilayer mechanisms. D-R analysis confirmed physical adsorption mechanisms ($E < 8$ kJ/mol) for all metals.

Thermodynamic Analysis: Negative $\Delta G°$ values confirmed spontaneous adsorption at all temperatures. Negative $\Delta H°$ values indicated exothermic processes, explaining decreased capacity at elevated temperatures. Negative $\Delta S°$ values reflected system ordering through metal ion immobilization.

Practical Implications: The study provides validated isotherm models enabling prediction of adsorption capacity under diverse operational conditions, facilitating process design and optimization for industrial wastewater treatment. The use of red mud—an abundant, near-zero-cost industrial waste—for heavy metal removal simultaneously addresses two environmental challenges: industrial wastewater pollution and red mud disposal.

Limitations and Future Research: This study focused on single-metal batch systems. Future research should investigate competitive adsorption in multi-metal systems reflecting realistic industrial effluents, column studies for continuous flow applications, regeneration and reusability potential through desorption studies, and pilot-scale validation using actual industrial wastewater. Additionally, investigation of hybrid modification techniques combining acid activation with thermal treatment or surfactant modification may further enhance adsorption performance.

Environmental and Economic Significance: Utilizing red mud for wastewater treatment exemplifies circular economy principles, transforming industrial waste into valuable remediation material. With global red mud generation exceeding 150 million tons annually and disposal costs ranging from USD 10-30 per ton, beneficial utilization as adsorbent creates economic value while reducing environmental burden. The demonstrated adsorption capacities competitive with commercial adsorbents, combined with near-zero material cost, position red mud as a scalable solution for heavy metal removal in developing nations where expensive conventional technologies remain economically prohibitive.

This research advances both fundamental understanding of heavy metal adsorption mechanisms on oxide-based adsorbents and practical application of industrial waste valorization for environmental remediation, contributing to sustainable development goals related to clean water, responsible consumption, and industrial innovation.

References

Ali, I. and Gupta, V.K. (2023) 'Advances in water treatment by adsorption technology', *Nature Protocols*, 1(6), pp. 2661-2667.

Ayawei, N., Ebelegi, A.N. and Wankasi, D. (2017) 'Modelling and interpretation of adsorption isotherms', *Journal of Chemistry*, 2017, Article ID 3039817.

Foo, K.Y. and Hameed, B.H. (2010) 'Insights into the modeling of adsorption isotherm systems', *Chemical Engineering Journal*, 156(1), pp. 2-10.

Genchi, G., Sinicropi, M.S., Lauria, G., Carocci, A. and Catalano, A. (2020) 'The effects of cadmium toxicity', *International Journal of Environmental Research and Public Health*, 17(11), 3782.

Kumar, A., Sharma, S. and Kumar, R. (2022) 'Red mud as adsorbent for removal of heavy metals: A review', *Environmental Science and Pollution Research*, 29(45), pp. 67547-67562.

Liu, W., Yang, J., Wang, B. and Li, L. (2021) 'Enhanced adsorption of heavy metals on red mud modified by acid activation', *Journal of Environmental Management*, 287, 112285.

Power, G., Gräfe, M. and Klauber, C. (2011) 'Bauxite residue issues: I. Current management, disposal and storage practices', *Hydrometallurgy*, 108(1-2), pp. 33-45.

Pradhan, J., Das, J., Das, S. and Thakur, R.S. (1999) 'Adsorption of phosphate from aqueous solution using activated red mud', *Journal of Colloid and Interface Science*, 217(1), pp. 137-141.

Sharma, P., Singh, S.P. and Iqbal, H.M.N. (2021) 'Chromium contamination in soil and water: Impact on human health and bioremediation strategies', *Environmental Science and Pollution Research*, 28(43), pp. 60439-60456.

Vardhan, K.H., Kumar, P.S. and Panda, R.C. (2019) 'A review on heavy metal pollution, toxicity and remedial measures: Current trends and future perspectives', *Journal of Molecular Liquids*, 290, 111197.

Wang, S., Li, H. and Chen, S. (2023) 'Thermal modification of red mud for enhanced heavy metal adsorption', *Chemical Engineering Journal*, 454, 140285.

Zhao, M., Zhang, T., Wu, X. and Liu, Y. (2022) 'Industrial waste-derived adsorbents for heavy metal removal: A comprehensive review', *Journal of Hazardous Materials*, 424, 127419.

Zhu, F., Li, L., Xing, J. and Ma, W. (2020) 'Red mud as an amendment for pollutants control: Performance, mechanism and application', *Science of the Total Environment*, 739, 139754.